# Thermal extraction of volatiles from the lunar regolith simulant NU-LHT-2M: preparations for in-situ analyses on the Moon

Journal Item

# Accepted Manuscript


Thermal extraction of volatiles from the lunar regolith simulant NU-LHT-2M: preparations for in-situ analyses on the Moon

P. Reiss, L. Grill, S.J. Barber

| | |
|---|---|
| PII: | S0032-0633(18)30382-9 |
| DOI: | 10.1016/j.pss.2019.05.001 |
| Reference: | PSS 4666 |
| To appear in: | *Planetary and Space Science* |
| Received Date: | 26 October 2018 |
| Accepted Date: | 03 May 2019 |

Please cite this article as: P. Reiss, L. Grill, S.J. Barber, Thermal extraction of volatiles from the lunar regolith simulant NU-LHT-2M: preparations for in-situ analyses on the Moon, *Planetary and Space Science* (2019), doi: 10.1016/j.pss.2019.05.001

# Thermal extraction of volatiles from the lunar regolith simulant NU-LHT-2M: preparations for in-situ analyses on the Moon

P. Reiss[1], L. Grill[2] and S.J. Barber[3]

[1]*Post-doctoral researcher, Technical University of Munich, Institute of Astronautics, Boltzmannstr. 15, 85748 Garching, Germany (p.reiss@tum.de)*

[2]*Research assistant, Technical University of Munich, Institute of Astronautics, Boltzmannstr. 15, 85748 Garching, Germany*

[3]*Senior Research Fellow, The Open University, School of Physical Sciences, Milton Keynes, MK7 6AA, United Kingdom*

**Abstract**

The present work describes the end-to-end demonstration of enriching the lunar highland regolith simulant NU-LHT-2M with loosely adsorbed water, releasing this and other volatile compounds by thermal treatment in high-vacuum, and identifying the released volatile species through mass spectrometry. This demonstration was performed to characterise how different sample conditions will affect the in-situ measurements performed by the ProSPA gas analysis instrument that is to operate at the lunar south pole on board the Russian Luna-27 lander. A laboratory breadboard was set up that allows testing of variable parameter combinations, such as different initial water contents, particle sizes, quantities, and bulk densities of the sample, as well as different heating rates. Three distinct temperature-dependent phases of outgassing were identified. Between -50 °C and 300 °C loosely adsorbed volatiles, mainly water in a mass fraction of around 0.1 % to 0.2 %, were released from the samples. Above that the samples showed mineral decomposition which led to the release of trapped water, carbon dioxide, and hydrogen sulfide. It was shown that the gas pressure produced by outgassing of the volatile species in a continuously pumped system is noticeably higher if the sample is larger, contains smaller particles, or if a higher heating rate is applied.

## 1 Introduction

The European Space Agency is developing the instrument package PROSPECT (Platform for Resource Observation and in-Situ Prospecting for Exploration, Commercial exploitation and Transportation) as a contribution to the Luna-27 mission of the Russian space agency Roscosmos. Luna-27 is scheduled to land in the south pole area of the Moon by 2023. PROSPECT consists of the drilling and sampling system ProSEED (PROSPECT Sample Excavation and Extraction Drill) and the sample analysis instrument ProSPA (PROSPECT Sample Processing and Analysis) (Barber et al. 2018; Carpenter et al. 2017). ProSPA receives potentially ice-bearing regolith samples from the drill, transfers them into sample ovens, and seals the latter by means of a so-called tapping station. Similar to other gas analysis instruments for planetary exploration (Reiss et al. 2017; Wright et al. 2015), the volatile constituents in the sample are extracted via continuous heating at predefined rates or by stepped heating. For the evolved gas analysis an ion trap mass spectrometer is used, while in a different operating

mode a magnetic sector mass spectrometer is used for a more detailed isotopic analysis of the released volatiles. In support of the instrument development the process of volatiles extraction was theoretically studied and analysed through simulations by Reiss (2018a). It was found that the initial water content of the sample can qualitatively be derived from the amplitude and time-dependency of the pressure that is produced in a dynamic system with constant vacuum pumping by the release of the volatile content. Furthermore, the effect of bulk density, heating rate, and thermal properties on the outgassing profile was investigated. In the work described here a test facility has been developed and built at the Technical University of Munich, with the goal to verify these theoretical results and to perform a proof of concept for the volatiles extraction process with a ProSPA-like configuration. The setup includes a conditioning system for the preparation and controlled hydration of regolith samples, and a volatiles extraction system for subsequent thermal processing of the samples under high-vacuum conditions and analysis of the evolved gases.

## 2 Experimental Setup

### *2.1 Sample Conditioning System*

The experimental setup for the preparation of lunar regolith simulants is depicted in Figure 1. It consists of a stainless steel glovebox (internal volume 0.8 m³) with purge gas feed, humidification/dehumidification system, and an attached vacuum airlock with a separate heater setup for sample bake-out. The humidity inside the glovebox is controlled through purging with nitrogen of purity 5.0 (99.999 % pure), which is either fed directly into the glovebox for dehumidification or guided through a bubbler with distilled water for humidification. Temperature and humidity are measured inside the glovebox near the sample with two independent sensors. A Sartorius Excellence E 1200 S precision balance (readability 0.001 g, standard deviation 0.001 g) is used for weighing the samples inside the glovebox. The airlock is equipped with a pressure gauge, evacuation line, and a D-Sub feedthrough for thermocouple and power supply. For bake-out under vacuum in the airlock, the sample is placed inside a borosilicate glass container and then mounted on top of a steel block that is heated from the inside via an inserted cartridge heater.

Figure 1: Glovebox with vacuum airlock for sample preparation

## *2.2 Volatiles Extraction System*

The experimental setup for the thermal extraction of volatiles from the sample consists of an instrumented vacuum system with two sections (Figure 2 and Figure 3). The lower part of the system is constructed using Swagelok ¼" tubes and VCR-type fittings. It includes the sample holder, a purge gas feed, a Leybold PTR 90 N pressure gauge, and a cooling/heating system that is applied externally to the sample holder (Figure 4). The upper part consists of CF40 vacuum tubes and contains a quadrupole mass spectrometer (Stanford Research Systems RGA 200, range 1 amu to 200 amu) and a second PTR 90 N pressure gauge. Both sections are connected via a manual dosing valve, which acts as an orifice to restrict the mass flow so that the RGA filament can be operated below its maximum gas pressure of $10^{-4}$ mbar. The operating pressure of the lower section is on the order of $10^{-8}$ mbar. The entire system is evacuated with an oil-free scroll pump (Leybold Scrollvac SC 5 D) as backing pump and a turbomolecular pump (Leybold Turbovac SL 80) for high vacuum. To avoid condensation of volatiles and enable a full bake-out, the system can be heated to 120 °C using heating wires wrapped around the tubes and insulated with aluminium foil. Temperature is measured at five locations throughout the system: at the sample holder, lower crosspiece, dosing valve, upper crosspiece, and upper pressure gauge.

The sample holder is a modified stainless steel blind fitting (Figure 4) to accommodate a sample of up to 2.8 mm in diameter and 4.5 mm in height, which is equivalent to the early ProSPA baseline sample size (Reiss et al. 2017). The sample holder is sealed towards the lower crosspiece with a steel gasket that holds a sintered filter with an average pore size of 60 µm to prevent dust particles escaping into the upper part of the vacuum system.

Because the sample holder should be removed, cleaned, and stored in the glovebox between the individual test runs, a detachable heater had to be designed. Following the design developed for previous studies (Reiss et al. 2017), a Macor ceramic heater mount was manufactured as depicted in Figure 4. For heating, a 0.2 mm diameter Kanthal A1 heating wire (32 AWG, 46.2 Ω/m, total length ~0.3 m) was initially chosen. After repeated mechanical

failure due to thermal cycling it was replaced after some tests with a thicker 0.25 mm diameter Kanthal A1 heating wire (30 AWG, 29.3 Ω/m, total length ~0.3 m), which proved to be more robust. A 0.5 mm diameter Type K mantle thermocouple was inserted into the heater to measure the temperature of the sample holder.

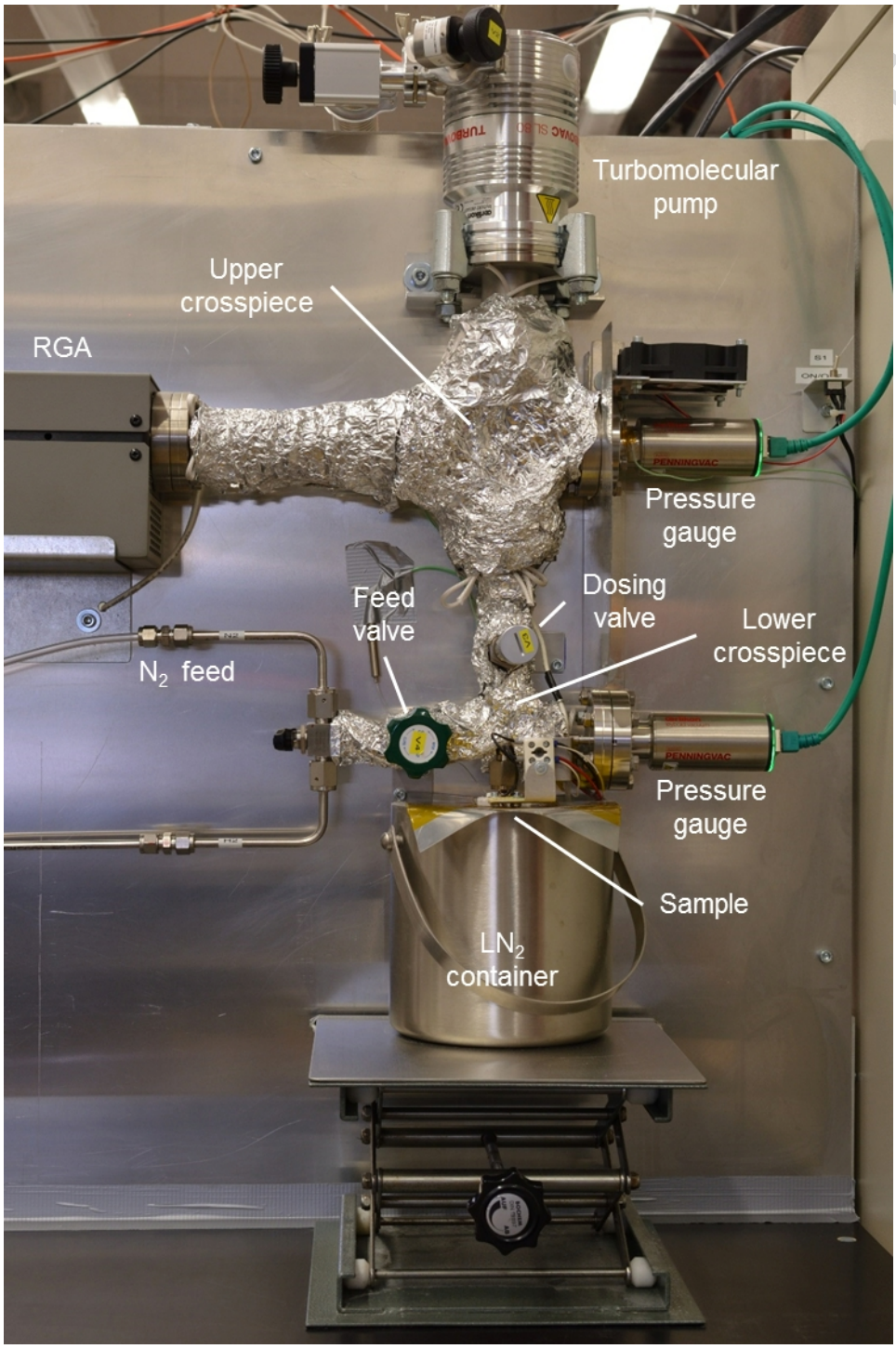


Figure 2: Volatiles extraction system

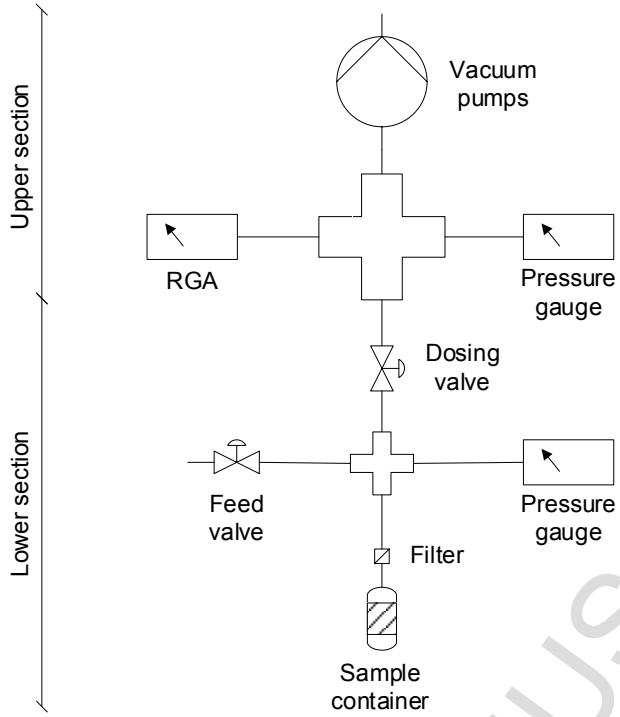


Figure 3: Schematic depiction of the volatiles extraction system

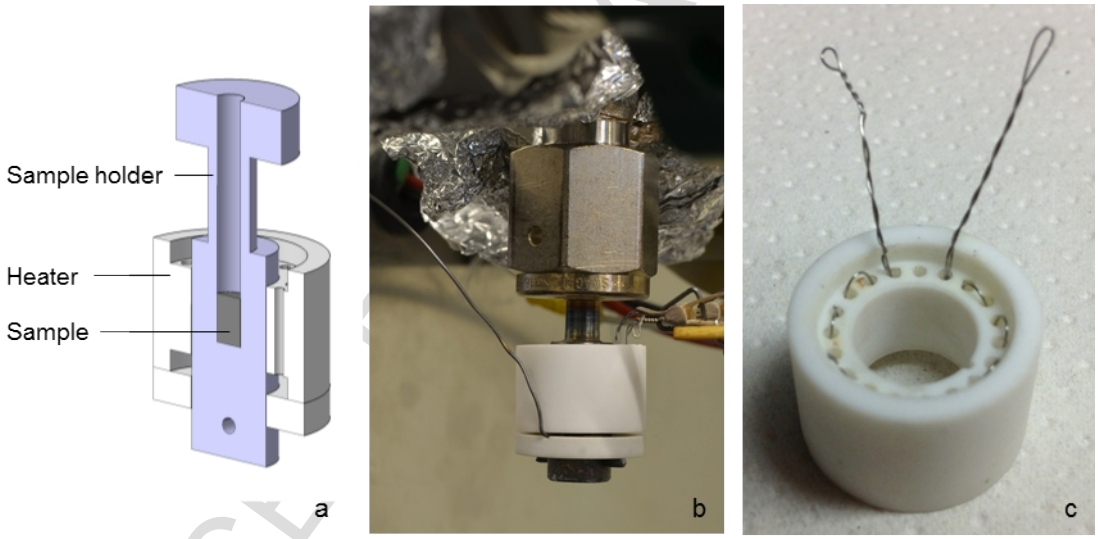


Figure 4: Detail view of the sample holder with heater: a) schematic sectional view, b) installed in volatiles extraction system, c) ceramic heater with wire

## 3 Sample Hydration

Numerous methods of adding water to lunar regolith and its analogues are described in the literature, including mixing the regolith with liquid water (Kleinhenz and Linne 2013) or hydrated mineral salt (Kleinhenz et al. 2008), adding water vapour or dispersed water to regolith (Pitcher et al. 2016), exposing regolith to a humidified carrier gas (Fuller and Agron 1976; Holmes and Gammage 1975; Robens et al. 2007), and injecting water vapour into an evacuated chamber with regolith (Beck et al. 2010; Poston et al. 2013). A review of these methods (Reiss 2018b)

concluded that exposing regolith to a humidified carrier gas is the most promising approach to achieve a controlled hydration of lunar regolith simulants with water mass fractions in the range of 0.1 % to 1 % by relatively simple means. The initial goal of the sample conditioning study presented here was to prove the feasibility of this process and applicability of the experimental setup for hydrating the lunar highland regolith simulant NU-LHT-2M (U.S. Geological Survey 2008). A further goal was the determination of how quickly the adsorption can be achieved with this process.

After some initial tests a long-term experiment was conducted where a sample was exposed to relative humidity levels between 1 % and 70 % in the glovebox. An OHAUS Discovery DV215CD precision balance with a readability of 0.01 mg was placed inside the glovebox to measure the mass gain of the sample during adsorption. A thin layer of NU-LHT-2M in its standard particle size distribution (Zeng et al. 2010) was spread over a stainless steel petri dish with 75 mm diameter and baked-out at >100 °C for 4 h under continuous vacuum pumping and a pressure of approximately $10^{-1}$ mbar. The sample was then transferred into the humidity-controlled volume of the glovebox and left there for at least 12 h and up to 48 h to adsorb water from the glovebox atmosphere at 1 % relative humidity. It was weighed two to three times over this duration until no further change in mass was noticeable. The relative humidity was then increased to 70 % in 10 % increments and the sample weighed two to three times at each step. For reference, the same procedure was conducted with an empty petri dish, for which the measured mass change in the humidified atmosphere was always <0.460 mg (<0.015 % of the sample mass) and therefore can be neglected.

Figure 5 shows the mass gain of the sample in the humidified atmosphere, normalised to the mass at the initial relative humidity (2.97838 g at 0.9 % relative humidity). The highest mass gain is visible in the step between 0.9 % and 10 % relative humidity, while towards 60 % relative humidity the mass gain seems to approximate saturation, but then deviates again from this trend at 70 % relative humidity. Two curve fits were applied to the data to find out whether the mass gain tends to saturate or grow further above 70 % relative humidity. Saturation is represented by a Type I Langmuir adsorption isotherm of the following form (Hill 1977):

$$q = q_{max}\frac{K \cdot c}{1 + K \cdot c} \tag{3-1}$$

Type II adsorption, according to the Brunauer–Emmett–Teller (BET) model, extends the Langmuir isotherm to account for multilayer adsorption at higher concentrations:

$$q = q_{max}\frac{K \cdot c}{(c_{sat} - c)\left(1 + (K-1)\frac{c}{c_{sat}}\right)} \tag{3-2}$$

Equations (3-1) and (3-2) use the coverage $q$, monolayer coverage $q_{max}$, coefficient $K$, adsorbate concentration $c$,

and saturation concentration $c_{sat}$. The same relation however is applicable to the dependence of mass gain to water concentration in the atmosphere, or relative humidity respectively.

The curve fits from Figure 5 do not lead to a clear conclusion regarding the type of adsorption. However, a Type II adsorption yields a slightly higher coefficient of determination ($R^2 = 0.998$ versus $R^2 = 0.995$). This would be in agreement with the results of similar measurements made by Holmes and Gammage (1975), Fuller and Agron (1976), and Robens et al. (2007, 2008). Such behaviour would mean that a monolayer of water is formed up to approximately 55 % relative humidity, where $q_{max}$ with a mass gain of 0.13 % is reached, followed by adsorption in the form of multilayers. The mass of a monolayer depends on the available adsorption sites on the particles and hence the specific surface area (SSA). For Apollo samples with mean particle sizes between 41 µm and 99 µm the SSA lies in the range of 0.02 m²/g to 0.78 m²/g, with a typical value of 0.5 m²/g (Cadenhead et al. 1977; Carrier et al. 1991). For the simulant NU-LHT-1M with mean particle sizes between 120 µm and 147 µm the SSA ranges from 0.1 m²/g to 0.3 m²/g (Malvern Instruments 2007). The SSA of the NU-LHT-2M used in the adsorption experiments was not measured, but a mean particle size of 60 µm was determined by wet laser diffraction analysis using a Shimadzu SALD-2201 analyser. With the SSA and the diameter of a water molecule of 2.75 Å, the monolayer-equivalent mass of adsorbed water can be estimated, yielding a value of 0.025 % for the aforementioned Apollo samples with a SSA of 0.5 m²/g, corresponding to mean particle sizes around 60 µm (Reiss 2018a). This is about one order of magnitude less than the water mass fraction of 0.13 % derived above for the NU-LHT-2M used here, suggesting that its SSA must be about the same factor higher (assuming comparable adsorption mechanisms). This could be caused by a more irregular particle shape or a higher amount of fines in the investigated NU-LHT-2M sample. The only SSA found in a similar range for a comparable material was 8 m²/g for a micronized sample of the lunar regolith simulant JSC-1A, as used in experiments by Poston et al. (2013).

Given the limitation to only one investigated sample batch no general conclusion about the types of adsorption on NU-LHT-2M can be drawn at this point. Nevertheless, for the experimental studies on volatiles extraction the process of sample conditioning was demonstrated to be sufficiently appropriate to produce hydrated samples with a water mass contents in the range of 0.1 %.

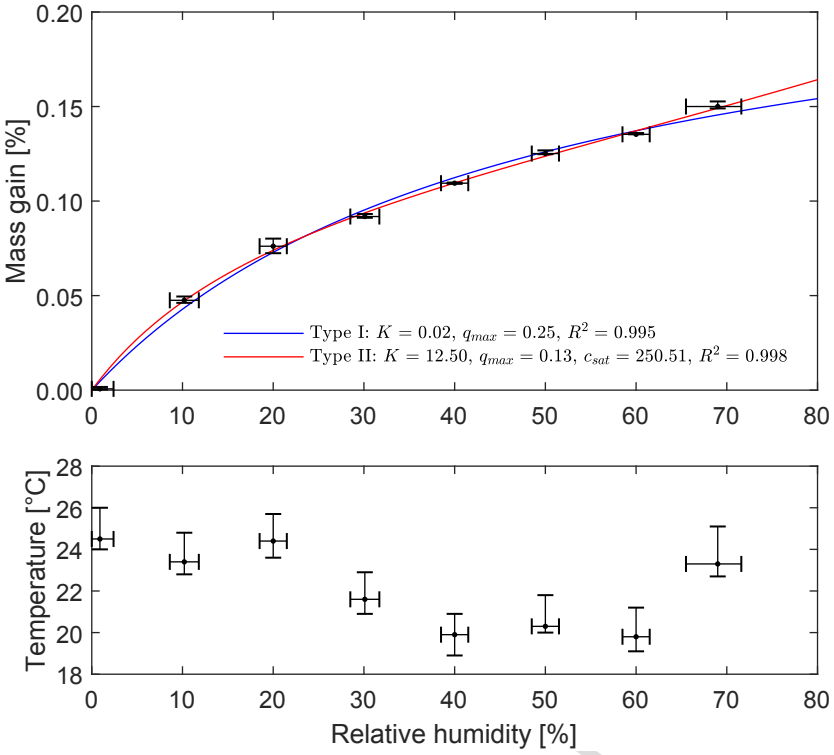


Figure 5: Mass gain and temperature over relative humidity for a long-time exposure of NU-LHT-2M to humidified nitrogen gas. Type I and II adsorption models were fitted to the mass gain data according to equations (3-1) and (3-2).

## 4 Volatiles Extraction

Variable parameters for the volatiles extraction experiments included the relative humidity during sample conditioning, sample mass, sample particle sizes, sample compaction, and heating profile, as listed in Table 1. At least three runs for each configuration were performed with additional reference measurements to record the background outgassing without sample.

Table 1: Test parameters for the volatiles extraction

| Parameter | Values |
|---|---|
| Relative humidity for hydration | 1 % / 10 % / 30 % / 50 % / 70 % / saturated |
| Sample mass | 33-36 mg / 66-72 mg |
| Particle size | 70-80 µm / 100-110 µm |
| Bulk density | loose (approx. 1.3 g/cm³) / compacted (approx. 2.0 g/cm³) |
| Heating mode | -190 °C to 800 °C at 6 °C/min / -190 °C to 800 °C at 4 °C/min |

For all tests the highland-type lunar regolith simulant NU-LHT-2M was used. The amount of water in the sample

was controlled by performing the previously described sample conditioning procedure in the glovebox at different levels of relative humidity between 1 % and 70 % (section 3 'Sample Hydration'). One additional set of saturated samples was created by mixing 6.66 g sample with 1 ml distilled water (15 % mass content), in accordance with saturation levels determined by Pitcher et al. (2016). The default sample mass for all runs was 33 mg to 36 mg, consistent with the ProSPA baseline sample size (27.7 $mm^3$) and a measured bulk density for loosely poured NU-LHT-2M between 1.2 $g/cm^3$ and 1.3 $g/cm^3$. An additional set of test runs with twice the amount of sample was also performed. The default particle size for the tests was 70 µm to 80 µm to represent the mean particle size of lunar regolith (Carrier et al. 1991). An additional set of runs with larger particles between 100 µm and 110 µm was also performed. The simulant NU-LHT-2M was manually sieved to obtain these particle size fractions. The sample was loosely filled into the sample holder and carefully tapped to ensure that all the sample rested at the bottom of the holder. A set of more compacted samples was also investigated, where a metal rod was used to press the sample while tapping against the sample holder, yielding a bulk density of approximately 2.0 $g/cm^3$, as determined by measuring the compacted volume and weighing the sample. By default the samples were heated from around -190 °C to 800 °C. The lower temperature limit was dictated by the temperature of the liquid nitrogen bath in which the sample holder was immersed. For the analysis of the experimental results presented here only measurement data above a sample temperature of -150 °C were considered, mainly because the expected minimum environmental temperature for ProSPA is around -150 °C. Another reason is that with the given setup the heater control was not sufficiently accurate at temperatures below -150 °C. The heating rates were chosen to be 6 °C/min in the default test case and 4 °C/min in additional test runs to enable a comparison with experimental studies by Gibson and Johnson (1971) and Gibson and Moore (1972).

Bake-out of the samples was performed in the glovebox airlock between 100 °C and 200 °C at approximately $10^{-1}$ mbar for at least 2 h. Inside the glovebox the sample was kept in a constant atmosphere for at least 48 h to adsorb water, before it was packed inside the sample holder, sealed, and transferred through the airlock to the volatiles extraction system.

The volatiles extraction system was purged with dry nitrogen, evacuated, and baked-out at 120 °C (150 °C at the RGA) for about 1 h prior to installation of the sample holder. Sample heating was activated when the pressure in the lower section of the volatiles extraction system reached values $<10^{-4}$ mbar. The system was continuously evacuated for the entire duration of the experiment. The RGA constantly performed evolved gas analysis (EGA) for selected masses, including m/z 2, 18, 28, 32, and 44, at intervals of 3 s during sample heating.

### *4.1 Test Results*

For the following interpretation of RGA data it is assumed that all volatiles that are released from the sample travel

through the dosing valve to the RGA, so that the measurement of the RGA is representative of the gas release that would be measured directly at the surface of the sample. This in turn involves the assumptions that there is no loss through condensation or resorption in the vacuum system, no accumulation of gas before the dosing valve, and that the gas mixture does not change over the valve. Because the total gas pressures measured up- and downstream of the valve show the same trends with an offset of two orders of magnitude, it is concluded that no significant pressure build up at the valve would have occurred. Nevertheless, it is expected that the gas composition does change to some extent because of the different diffusivities of species in the vacuum system and through the valve. Due to the pressure restrictions of the RGA, the direct gas analysis in the lower section close to the sample was not possible, hence a more detailed analysis of this issue is not possible here. A certain influence of this issue on the RGA data must therefore be taken into account, such as peak broadening through increased residence times of evolved gases upstream of the valve.

Figure 6 shows a typical progression of partial pressures of the predominant masses detected by the RGA. For all parameter combinations in the experiments this typical diagram can be divided into three distinct phases: An initial peak (A) between -100 °C and -50 °C (phase 1), a broader feature (B) between -50 °C and 300 °C (phase 2), and two separately identifiable peaks (C-D) at temperatures above 300 °C (phase 3). These three phases are analysed in more detail in the following sections. From the mass spectra at peaks A-D (Figure 7) the prevailing species in the gas mixture can be clearly identified by their fragmentation pattern (major mass fragments underlined): $H_2O$ (m/z 16, 17, 18, 19, 20), $H_2$ (m/z 1, 2), and $CO_2$ (m/z 12, 16, 28, 44, 45, 46).

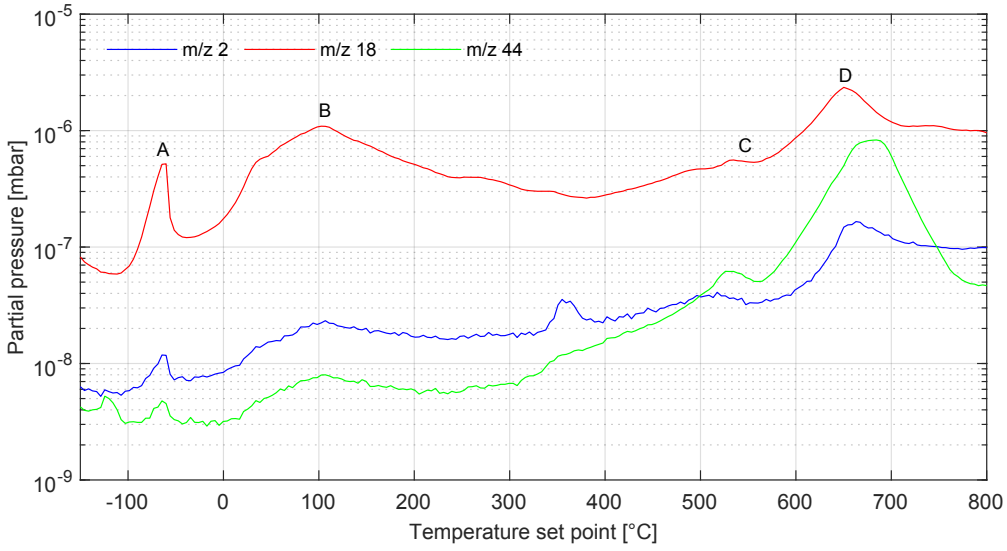


Figure 6: Exemplary partial pressure curves of selected species for the extraction of volatiles with 6 °C/min heating rate and a 33-36 mg, 70-80 µm, loose sample, conditioned at 30 % relative humidity

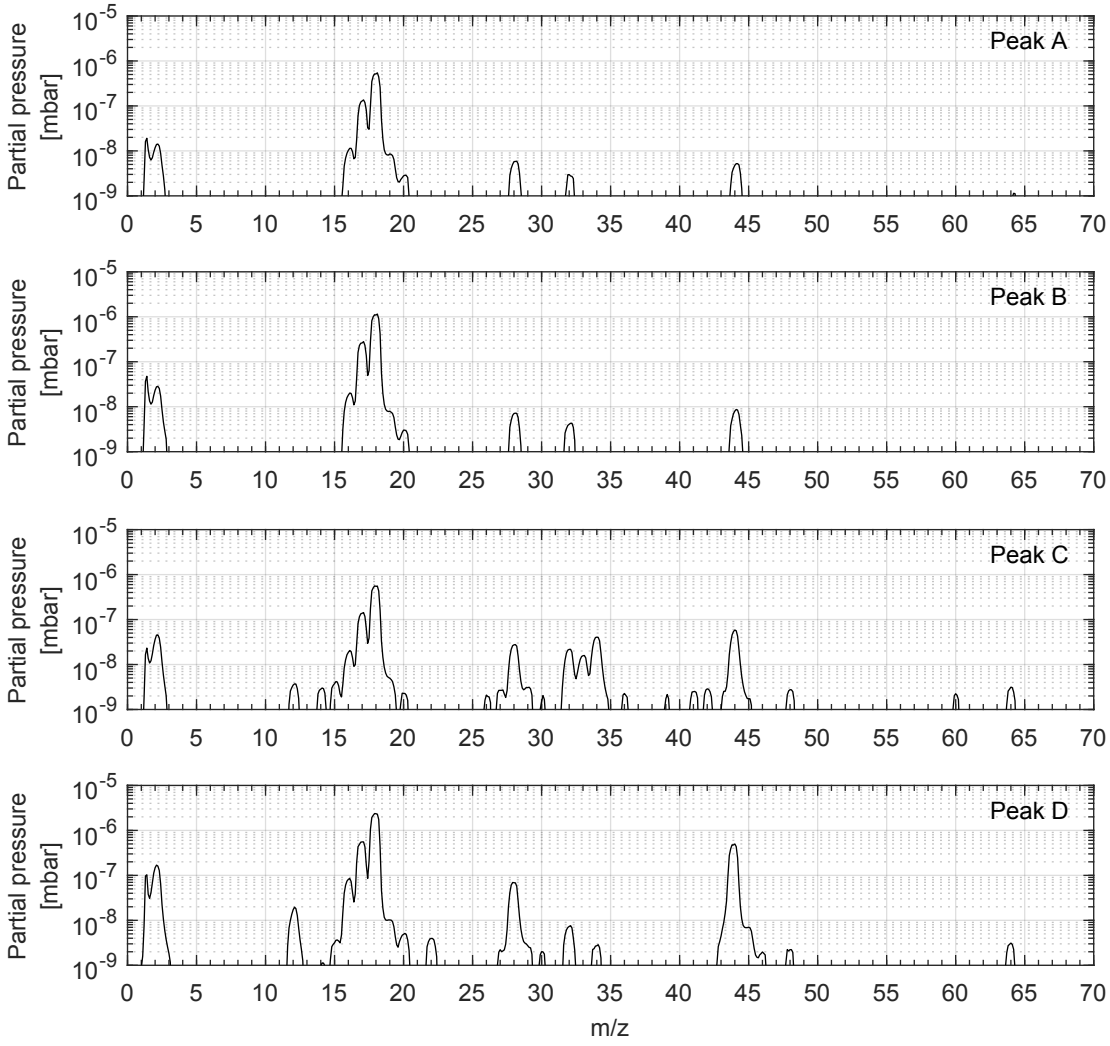


Figure 7: Exemplary mass spectra at selected outgassing peaks (see Figure 6) for the extraction of volatiles with 6 °C/min heating rate and a 33-36 mg, 70-80 µm, loose sample, conditioned at 30 % relative humidity

### *4.1.1 Phase 1: Temperature below -50 °C*

The first significant peak (A) was visible in all outgassing curves as well as in the reference runs without sample, but with a noticeable shift to higher temperatures and a higher amplitude (Figure 8). The outgassing feature is attributed to the desorption of atmospheric gases that are loosely bound to the internal steel surface of the sample holder and the upper surface of the sample. Because the surface area is higher for the empty sample holder, a higher quantity of gases can adsorb, thus producing a higher pressure when they desorb. The shift of the peak to higher temperatures in the case of the empty sample holder is explained with the additional time required for the surface to reach a sufficiently high temperature for desorption. When a sample was present the pressure rise started at a set point temperature around -120 °C to -110 C°, while for the empty sample holder the pressure rise started between -100 °C and -80 °C. As a thermal analysis of the test setup described in section '4.2 Thermal Analysis' showed, the upper surface of the sample receives heat both via radiation from the upper warmer part of the sample

225 holder and hence heats up faster than the rest of the sample (compare Figure 13). Because this happens faster than
226 the mainly conductive heating of the bottom internal surface of the empty sample holder, the outgassing peak
227 happens earlier when a sample is present.
228 The most probable cause for the initial outgassing peak is contamination of the glovebox atmosphere. Other
229 potential explanations, such as contamination in the volatiles extraction system, contamination of the filter gasket,
230 or contamination by ambient air during sample transfer from the glovebox to the vacuum system (Reiss 2018b),
231 were ruled out systematically through additional control runs.

232 *4.1.2 Phase 2: Temperature between -50 °C and 300 °C*

233 The second broad outgassing feature (B) is attributed to the outgassing of the volatiles that are loosely adsorbed
234 on the sample particles. Different sample conditions clearly have an effect on the shape and amplitude of this
235 outgassing feature between -50 °C and 300 °C, which is analysed in more detail in the following.
236 Initial water concentration
237 For the samples that were conditioned at relative humidity levels of 30 %, 50 %, and 70 %, no significant
238 difference in the outgassing peaks is noticeable (Figure 8a). Only minor deviations can be seen that most likely
239 are due to variations in the sample preparation process or the sample composition. The outgassing feature includes
240 two subsequent pressure rises, one between -50 °C and 0 °C and one between 50 °C and 100 °C. The sample
241 conditioned at 10 % relative humidity produces a slightly lower outgassing pressure, but within the same order of
242 magnitude compared to the samples stored at higher relative humidity. A strong difference however can be seen
243 for the samples conditioned at 1 % relative humidity, where the total gas pressure is almost one order of magnitude
244 lower. Furthermore the shape of the outgassing feature is different, showing only a single broad peak instead of a
245 double peak. From these results it can be hypothesised that the adsorption of volatiles, mainly water, is strongest
246 at relative humidity levels below 10 %. This is in partial accordance with the results of the adsorption study
247 presented above (compare section '3 Sample Hydration'**Error! Reference source not found.**), although the
248 further increase in adsorbed water above this humidity level cannot be clearly identified through the volatiles
249 extraction studies.
250 Particle size
251 The amplitude of the pressure created by the outgassing of the more coarse-grained sample is generally lower than
252 for the fine-grained sample (Figure 8b). This was expected because of the smaller specific surface area and hence
253 less adsorbate. The pressure produced with the larger fraction also shows more pronounced peaks and more rapid
254 pressure drops after each peak. This could be caused by the larger voids in the sample and hence a higher gas

255 diffusivity, assuming that tortuosity would remain similar or be lower at the same time.

256 Bulk density

257 Compared to the loose sample, the compacted sample produces a widely similar pressure curve with similar
258 amplitude and only slightly more pronounced peaks (Figure 8c). With the given experiment, no distinctly different
259 outgassing behaviour is visible from the two investigated bulk densities. Theoretical analysis by Reiss (2018a)
260 predict a 50 % lower gas diffusivity when increasing the bulk density from 1.3 g/cm³ to 2.0 g/cm³, while the
261 thermal diffusivity is less for the higher compaction in the present temperature range. As a result, the features in
262 the outgassing curves should be delayed, or shifted to higher set point temperatures respectively. However, the
263 existing uncertainties in the experimental procedure apparently obscure the effects of sample compaction. Another
264 possible cause is sample disturbance during evacuation, that is, the compacted samples loosen up when giving way
265 to the escaping residual gas in the voids, leading to a similar compaction after evacuation than the non-compacted
266 samples.

267 Sample size

268 The outgassing of the larger sample mass produces a pressure that is generally and up to two times higher than the
269 one of the smaller sample (Figure 8d). The initial peak (compare peak labelled ‘A’ in Figure 6) is significantly
270 shifted towards lower temperatures, or earlier times respectively, which presumably is because less of the internal
271 surface of the sample holder is exposed due to the higher filling height. Other than that, the shape of the pressure
272 curve is quite comparable for both investigated sample sizes.

273 Heating rate

274 Reducing the heating rate from 6 °C/min to 4 °C/min has a similar effect on the general appearance of the
275 pressure curve as the larger particle fraction (Figure 8), in a way that the amplitude is lower and the features are
276 more pronounced. As shown in simulations by Reiss (2018a), the gas pressure inside the sample is lower when
277 reducing the heating rate, because a smaller quantity of desorbed volatiles can accumulate due to smaller
278 temperature gradients in the sample.

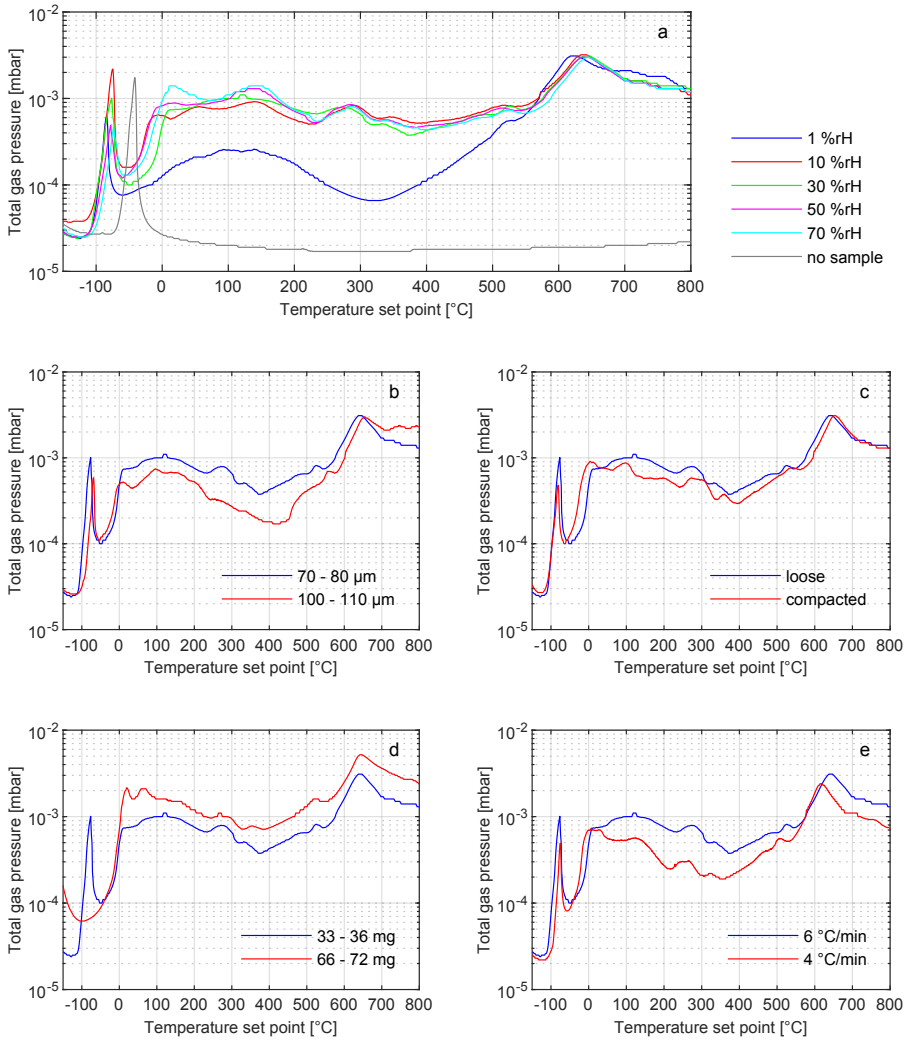


279

280 Figure 8: Comparison of total gas pressures near the sample for different parameter combinations (selected curves): a) different relative
281 humidity during sample conditioning, b) different particle size, c) different compaction, d) different sample size, e) different heating rate.

282 Volatiles yield

283 To evaluate how much water was actually added to the sample during the sample conditioning process, a simple
284 attempt to relate the rate of gas release to the total yield via integration over time is presented in the following.
285 The amount of species removed from the sample over time $n_i(t)$ can be calculated with the ideal gas law when
286 replacing the gas volume with a constant pump rate $q_{pump}$:

$$n_i(t) = p_i(t) \cdot \frac{q_{pump}}{R \cdot T} \tag{4-1}$$

287 Where $p_i(t)$ is the partial pressure of the individual species, $R$ is the universal gas constant, and $T$ is the
288 temperature. To simplify the computation, a constant evacuation with $q_{pump} = 65\ l/s$ was assumed, matching the

289 value for $N_2$ (60 l/s for Ar, 55 l/s for He, and 49 l/s for $H_2$) provided by the manufacturer (Leybold GmbH 2009).
290 While the pump rate is not constant at higher pressures, it was deemed sufficiently constant at the given high-
291 vacuum conditions. The temperature of the gas mixture was assumed to be 120 °C, equalling the temperature of
292 the heated pipes of the vacuum system. Integrating equation (4-1) over time and multiplying with the respective
293 molar mass $M_i$ the total mass $m_i$ of each species can be calculated:

$$m_i = M_i \int n_i(t) \tag{4-2}$$

294 This approach can only yield indicative values for the gas masses, since it implies major simplifications.
295 Nonetheless, it allows a relative comparison and a qualitative conclusion about the effectiveness of the sample
296 preparation procedure.
297 The computation was performed for all test runs in the temperature range from -150 °C to 300 °C to account for
298 the extracted volatiles during phase 2 only. The gas masses determined for the reference runs without sample were
299 subtracted to calculate the net gas masses for each test run. The samples with default particle size and mass (70 µm
300 to 80 µm, 33 mg to 36 mg), conditioned at a relative humidity between 10 % and 70 %, yielded a mass content of
301 m/z 18 between 0.2 % and 0.3 %. The mass of the remaining gases in the mixture was about one order of magnitude
302 less. Note that m/z 18 makes up 74 % of the fragments of water, so accounting for the other fragments would yield
303 slightly higher masses for water. The compacted sample and the sample with twice the mass yield a slightly lower
304 amount of released m/z 18, which could be due to a lower diffusivity, meaning that not all desorbed volatiles had
305 enough time to leave the sample until 300 °C was reached. The larger particle fraction yielded a significantly lower
306 mass content of m/z 18, between 0.1 % and 0.2 %. This is reasonable given the lower specific surface area of the
307 larger particles and hence less adsorbate. Generally, it is noteworthy that the amounts of water derived with the
308 simplified calculation approach described above are in the same order of magnitude as the amounts of adsorbed
309 water that were found in the adsorption study presented in section 3 ‘Sample Hydration’.
310 Regarding the saturated samples that were investigated here the yield of m/z 18 in terms of mass amounts to only
311 6 % at maximum, with large deviations between the test runs. It was concluded that the deviation mainly originated
312 from an inhomogeneous mixture of the sample with distilled water, rather than evaporation or other factors. The
313 procedure to create the saturated samples was to mix a larger sample quantity with a mass fraction of 15 % distilled
314 water in the glovebox, place three subsamples in separate sealed glasses and leave them for approximately 66 h
315 before taking a 33 mg to 36 mg portion out for the tests runs on four subsequent days. On the fourth day a second
316 portion was taken from the first subsample to check for any time dependency of the water content. However, test
317 run 1 and 4 yielded a mass fraction of 6.2 % and 6.3 % for m/z 18 respectively, so this was not the case. In contrast
318 to that test run 2 and 3 yielded only 3.4 % and 0.4 % for m/z 18 respectively. The internal volume of the glass

containers in which the sample were stored in could take up about 2 mg of water at saturation under the given conditions in the glovebox (temperature of 25 °C and saturation pressure of 3161 Pa, as calculated with the suggested Magnus equation from Alduchov and Eskridge (1996)). This represents around 3 % of the sample mass, which partly explains the deviation from the initially measured 15 %.

### *4.1.3 Phase 3: Temperature above 300 °C*

For all parameter combinations, the partial pressures as well as the total gas pressure show a very similar trend at temperatures above 300 °C. It is assumed that outgassing is caused by volatiles released from mineral decomposition rather than from surface desorption. Similar conclusions were drawn by Street et al. (2010), ten Kate et al. (2010), and Glavin et al. (2012), who measured a release of $CO_2$, $SO_2$, $H_2S$, and S between 300 °C and 600 °C.

Table 2 lists the major mineral phase abundances of NU-LHT-2M for particles with a single phase (99.2 % of all particle compositions are a single phase). According to Street et al. (2010) the source material of NU-LHT-2M has undergone hydrothermal alteration, which could explain the release of trapped $H_2O$ at higher temperatures. The occurrence of sulfur- and carbon-bearing species is discussed in the following.

Table 2: Major mineral phase abundances in NU-LHT-2M according to Rickman and Lowe**rs (2012)**

| Mineral | Volume across all particle size fractions [%] | Volume in 75 µm - 150 µm fraction [%] |
|---|---|---|
| Plagioclase | 62 | 59 |
| Glass | 18.7 | 17.3 |
| Clinopyroxene | 5.6 | 3 |
| Orthopyroxene | 5.6 | 8.3 |
| Olivine | 4.5 | 6.6 |
| Chlorite | 1.7 | 2.3 |
| Ilmenite | 0.6 | 1.5 |
| Quartz | 0.4 | 0.3 |
| Albite | 0.4 | 0.9 |
| Total | 99.5 | 99.2 |

Sulfur-bearing species

In the experiments presented here, a significant peak in the m/z 32 signal was detected around 550 °C. This was mainly attributed to $H_2S$ (fragments m/z 1, 32, 33, 34, 35, 36) and traces of $SO_2$ (fragments at m/z 16, 24, 32, 48, 50, 64, 65, 66), which have a very similar trend (Figure 9). While m/z 34 is also a (isotopic) fragment of oxygen, its relative abundance was much higher than to be expected for oxygen ($O_2$ fragments are 89 % m/z 32 and <1 %

m/z 34). The second major fragment of oxygen, m/z 16, follows the curves of m/z 18 and m/z 44 much more than m/z 32 and m/z 34, suggesting that there is no significant amount of oxygen present. $H_2S$ is assumed to have formed from sulfur released by decomposition of the sample and hydrogen in the gas mixture. This is supported by the fact that there is a visible drop in the hydrogen partial pressure at the same temperatures at which $H_2S$ is detected. According to analyses by Rickman and Lowers (2012), NU-LHT-2M contains traces of the mineral pyrite ($FeS_2$), which could be the source of sulfur in this case. Hydrogen reduction of pyrite is a well-known process (e.g. Lambert et al. 1998), in which sulfur is thermally released, diffuses through the $FeS_2$ layer to the particle surface, and is removed by hydrogen. Because the removal by hydrogen is faster than the mere desorption of sulfur, the overall reduction is more rapid when hydrogen is present.

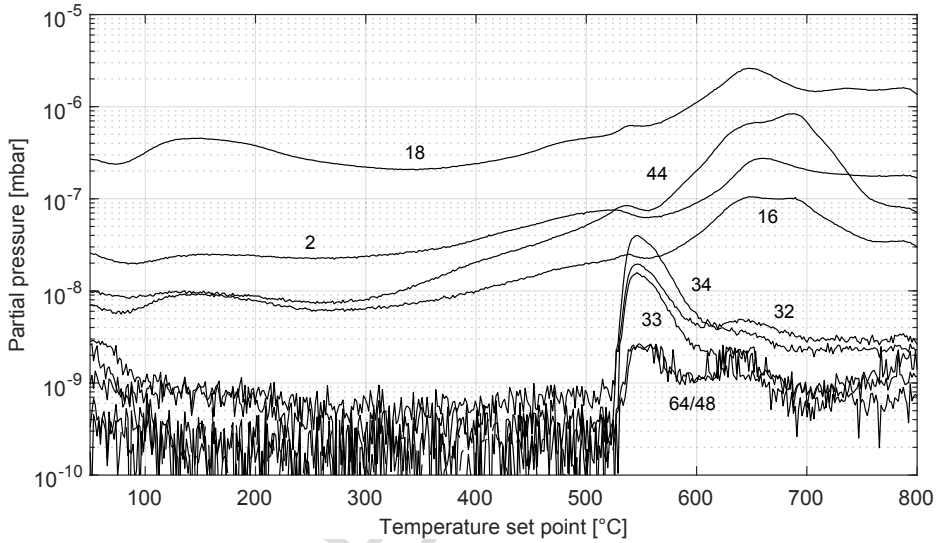


Figure 9: Evidence for the decomposition of sulfur-bearing minerals (numbers indicate the m/z ratio of the depicted species; major fragments of $H_2S$ are shown in colour)

Carbon-bearing species

As shown in Figure 6, a significant amount of carbon-bearing species was released from the sample at temperatures above 300 °C. This was mainly noticeable through a major peak of m/z 44 at 650 °C, which could be identified to be carbon dioxide due to the similar trends and matching abundances of its other major fragments m/z 28 and m/z 12. The search for a possible source of carbon in the simulant NU-LHT-2M yielded that it contains traces of the mineral calcite ($CaCO_3$), with <0.3 vol% in the fractions <150 µm, predominantly in the fraction from 75 µm to 150 µm (Rickman and Lowers 2012). Calcite originates from alteration of the source material for NU-LHT-2M and due to the imperfectness of the manual sorting process traces of this unintentional constituent are present in the simulant. To investigate whether the carbon dioxide had formed from carbon in the mineral or any other contamination, additional tests were performed where it was attempted to remove the carbon minerals from the

362 sample before testing. This was performed through washing with distilled water, which would remove particulate
363 biological contamination, and hydrochloric acid (HCl) to dissolve and remove minerals such as calcite. HCl
364 treatment of the sample was done using a 1 mol/l dilution with subsequent decanting and two times rinsing with
365 distilled water.
366 Figure 10 shows a comparison of partial pressures measured from test runs with differently treated samples. The
367 HCl-wash removes nearly all of the outgassing features attributed to carbon dioxide, supporting the hypothesis
368 that there was carbon-based contamination in the sample. However, the $H_2O$-wash also visibly alters the broad
369 double-peak outgassing feature of carbon dioxide such that the first peak around 650 °C is completely removed.
370 A closer investigation of the mixture of sample and water lead to a possible explanation of this effect. As shown
371 in Figure 11, the surface of the water was visibly clouded with fine particles after the rest of the sample had settled
372 at the bottom of the glass container. Some of the fine particles that accumulated at the water surface were pipetted,
373 dried, and investigated with a microscope. It was found that the particles had a diameter <5 μm and were present
374 as single particles or agglomerates, as depicted in Figure 11. The remaining regolith without these fine particles
375 was also subjected to the volatiles extraction procedure, which produced essentially the same curve as shown in
376 Figure 10 for the $H_2O$-washed sample. This strongly supports the hypothesis that the first carbon dioxide peak at
377 650 °C was caused by very fine particle residues in the sample. This also means that the sieving process was not
378 ideal and that such small residues potentially had affected all experiments presented above.

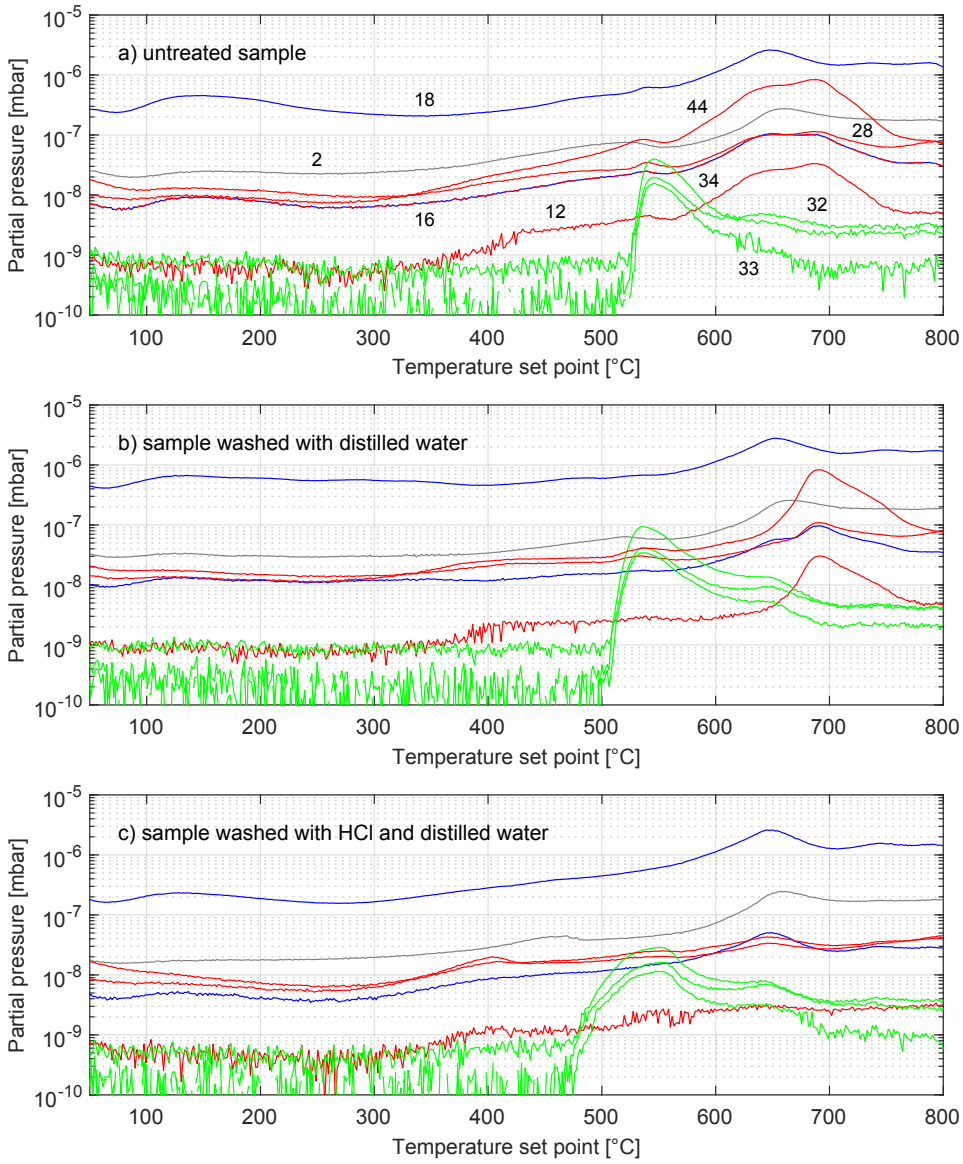


379

380 Figure 10: Effect of different sample treatments on the outgassing at higher temperatures. Selected species fragments are shown: $CO_2$ (red
381 curves with m/z 12, 16, 28, 44), $H_2O$ (blue curves with m/z 16, 18), $H_2S$ (green curves with m/z 32, 33, 34), and $H_2$ (grey curve with m/z 2).

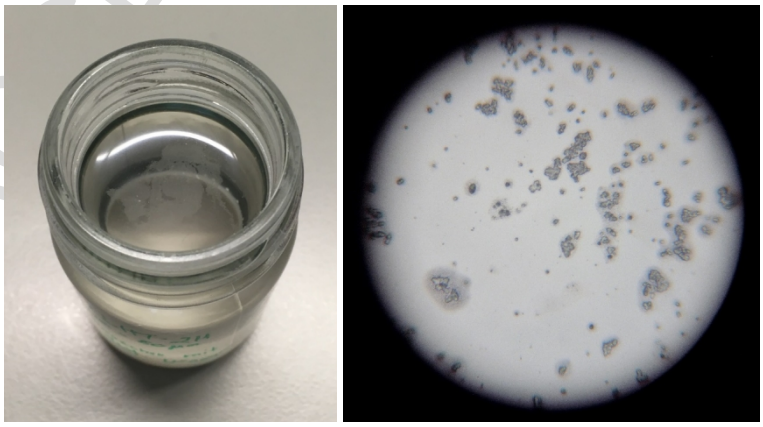

382

383 Figure 11: Mixture of distilled water with the 70 µm to 80 µm fraction of NU-LHT-2M with very fine-grained particles clouding the water
384 surface (left) and microscopic image of the dried particles collected from the water surface (right, particle diameters are <5 µm)

### *4.2 Thermal Analysis*

As highlighted in earlier studies (Reiss 2018a; Reiss et al. 2017), a significant thermal gradient within the sample can be expected under the given conditions. The set point temperature that was measured at the heater on the outside wall of the sample holder therefore has an offset to the temperatures that actually occur in the sample. To assess how significant this deviation is, a thermal model was set up to simulate the heat transfer in the sample holder. While the set point temperature was applied to the position of the thermocouple in the model, the lower crosspiece of the vacuum setup was programmed to follow a temperature progression from 150 °C to 190 °C over the test duration, as measured with a separate thermocouple during test.

The sample was modelled using a temperature- and pressure-dependent thermal model for NU-LHT-2M developed by Reiss (2018b) and a constant gas pressure of $10^{-5}$ mbar as a simplification. Figure 12 shows the resulting deviation of minimum, maximum, and average sample temperature from the temperature set point for a heating rate of 6 °C/min and 4 °C/min. Initially the thermal inertia of the sample leads to a large thermal gradient inside the sample of up to approximately 100 °C at around 0 °C set point for the higher heating rate. The positive deviation of the maximum sample temperature is caused by radiation from the warmer upper part of the sample holder. Although the thermal gradient is then continuously reduced over time, a permanent discrepancy of approximately 30 °C to 40 °C between average sample temperature and set point remains. Near a set point temperature of 250 °C, the radiative heat loss from the sample surface and the external surfaces of the sample holder leads to an even higher temperature gradient inside the sample, which further increases and reaches a maximum of approximately 150 °C at the end of the heating process.

The simulation highlights that the previously described outgassing features observed during the experiments need to be matched to temperatures that are about 30 °C to 40 °C on average lower than the set point. For the lower heating rate of 4 °C/min, the deviation of sample temperatures from the set point is not as high as for the higher heating rate, especially at set point temperatures up to 250 °C.

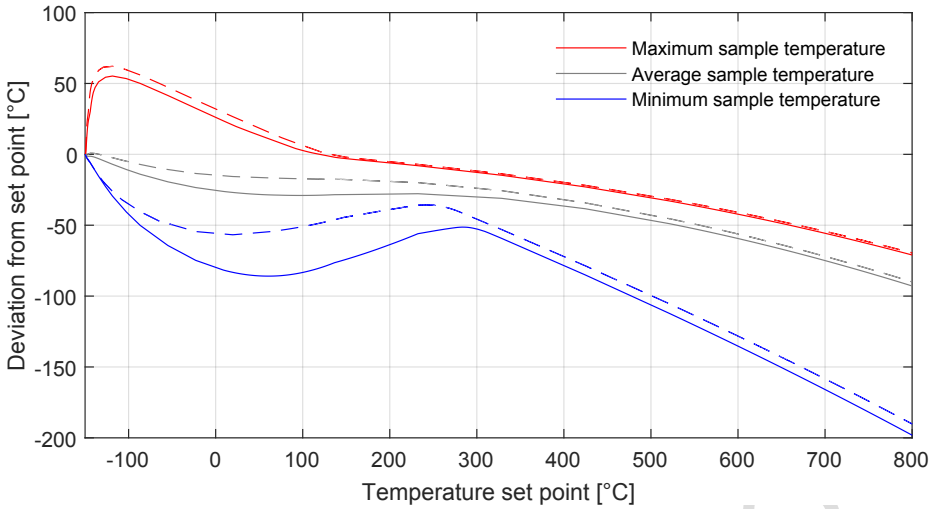


Figure 12: Simulated deviation of maximum, average, and minimum sample temperature from the set point for a heating rate of 6 °C/min (solid lines) and 4 °C/min heating rate (dashed lines).

Figure 13 shows the simulated temperature distribution in the sample holder during the first phase of heating, both with and without sample. In section '4.1.1 Phase 1: Temperature below -50 °C' it was discussed that the absence of a sample leads to a slower heating of the internal surface of the sample holder, thus delaying the initial outgassing peak that was attributed to atmospheric contamination of the sample holder. According to Figure 13, for a set point temperature of -120 °C (at the outer boundary of the sample holder), the upper few hundred micrometres of the sample already reach temperatures above the set point due to radiative heating from the warmer part of the sample holder above. At the same time the temperature at the bottom of the empty sample holder matches the set point temperature well. This finding also has further implications for the design of the experimental setup as well as the ProSPA instrument. While the upper part of the sample holder and the pipes that guide the released volatiles to the mass spectrometer need to be heated to avoid resorption and condensation, they need to be thermally decoupled from the sample holder as much as possible. The sample holder used here was modified to minimise the conductive heat transfer by reducing its wall thickness from 3 mm to 1 mm in the upper section. However, as shown by the thermal analysis this was not sufficient to avoid that the sample is thermally disturbed via radiation. Nevertheless, as the set point temperature increases the disturbing influence is compensated, which is visible through the decreasing deviation of the maximum sample temperature (upper sample surface) from the set point (Figure 12).

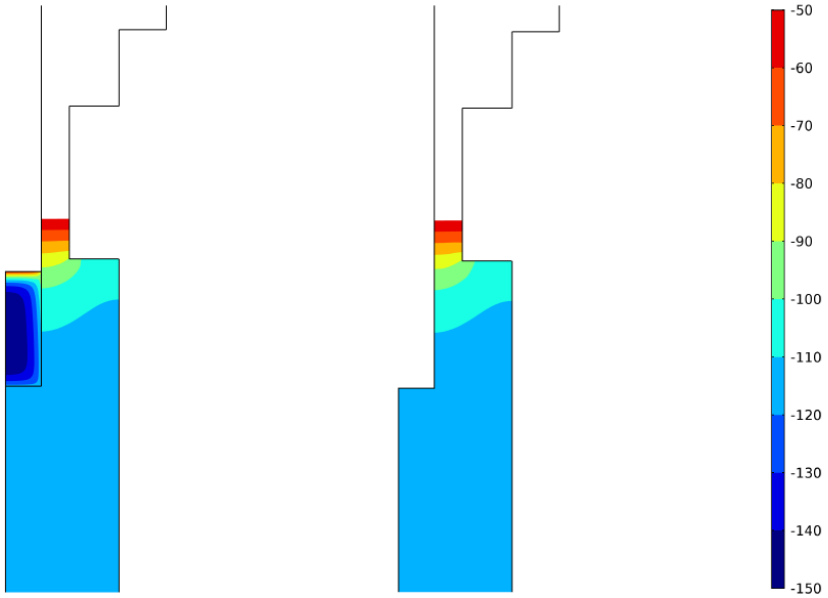


Figure 13: Simulated temperature distribution in the sample holder with (left) and without (right) sample. Only temperatures between -150 °C and -50 °C are displayed.

## Conclusions

This study describes a new experimental approach of hydrating the lunar regolith simulant NU-LHT-2M to achieve a water mass content around 0.1 % and thermally extracting volatile content from the simulant in high-vacuum at temperatures between -150 °C and 800 °C. It was found that NU-LHT-2M can be hydrated by storing it in a humidity-controlled nitrogen atmosphere for at least 12 h. With this approach water mass fractions of up to 0.15 % were added to the sample at a relative humidity of 70 %, while the relation between relative humidity and mass gain is nonlinear. The thermal extraction of the adsorbed volatiles in a dedicated breadboard of the ProSPA instrument setup was demonstrated and three distinct phases of outgassing were identified. Between -50 °C and 300 °C loosely adsorbed volatiles were released from the sample and characteristic relations between the sample conditioning parameters and the measured outgassing features could be drawn. It was found that samples with water mass content below 10 % produced different amplitudes of outgassing pressure, while for higher water contents the outgassing features were not clearly distinguishable. As a general trend, increased gas pressures from the release of volatiles were measured for a smaller particle fraction (70-80 µm instead of 100-110 µm), a larger sample mass (66-72 mg instead of 33-36 mg), and a higher heating rate (6 °C/min instead of 4 °C/min). Above 300 °C, mineral decomposition led to an increased outgassing activity, including the release of trapped water from hydrothermally altered minerals. Sulfur-bearing minerals in NU-LHT-2M were found to decompose above 550 °C and produce mainly $H_2S$, and traces of calcite in NU-LHT-2M were found to decompose above 650 °C and produce $CO_2$.

## Acknowledgements

The presented work was performed at the Institute of Astronautics at Technical University of Munich in support of the PROSPECT/ProSPA project. PROSPECT is a program of and funded by the European Space Agency.

## References

Alduchov, O. A., and Eskridge, R. E. (1996). "Improved Magnus form approximation of saturation vapor pressure." *J. Appl. Meteorol.*, 35(4), 601–609.

Barber, S., Wright, I., Abernethy, F., Anand, M., Dewar, K., Hodges, M., Landsberg, P., Leese, M., Morgan, G., Morse, A., Mortimer, J., Sargeant, H., Sheard, I., Sheridan, S., Verchovsky, A., Goesmann, F., Howe, C., Morse, T., Lillywhite, N., Quinn, A., Missaglia, N., Pedrali, M., Reiss, P., Rizzi, F., Rusconi, A., Savoia, M., Zamboni, A., Merrifield, J., Gibson, E., Carpenter, J., Fisackerly, R., Houdou, B., Sefton-Nash, E., and Trautner, R. (2018). "ProSPA: analysis of lunar polar volatiles and ISRU demonstration on the Moon." *49th Lunar Planet. Sci. Conf.*, 2172.

Beck, P., Pommerol, A., Schmitt, B., and Brissaud, O. (2010). "Kinetics of water adsorption on minerals and the breathing of the Martian regolith." *J. Geophys. Res.*, 115(E10), E10011.

Cadenhead, D. A., Brown, M. G., and Rice, D. K. (1977). "Some surface area and porosity characterizations of lunar soils." *Proc. 8th Lunar Sci. Conf.*, 1291–1303.

Carpenter, J. D., Fisackerly, R., ESA Lunar Exploration Team, PROSPECT User Group, and PROSPECT Industrial Team. (2017). "PROSPECT: ESA's package for resource observation and in situ prospecting for exploration, commercial exploitation and transportation." *Proc. Lunar Planet. Sci. Conf. XLVIII*, 2514.

Carrier, W. D., Olhoeft, G. R., and Mendell, W. (1991). "Physical properties of the lunar surface." *Lunar Sourceb.*, 475–594.

Fuller, E. L., and Agron, P. A. (1976). *The reactions of atmospheric vapors with lunar soil*.

Gibson, E. K., and Hubbard, N. J. (1972). "Thermal volatilization studies on lunar samples." *Proc. Third Lunar Sci. Conf.*, 2003–2014.

Gibson, E. K., and Johnson, S. M. (1971). "Thermal analysis-inorganic gas release studies of lunar samples." *Proc. Second Lunar Sci. Conf.*, 1351–1366.

Glavin, D. P., Malespin, C., ten Kate, I. L., Getty, S. a., Holmes, V. E., Mumm, E., Franz, H. B., Noreiga, M., Dobson, N., Southard, A. E., Feng, S. H., Kotecki, C. a., Dworkin, J. P., Swindle, T. D., Bleacher, J. E., Rice, J. W., and Mahaffy, P. R. (2012). "Volatile analysis by pyrolysis of regolith for planetary resource exploration." *Proc. 2012 IEEE Aerosp. Conf.*, IEEE, Big Sky, Montana, 1–11.

Hill, C. G. (1977). *An introduction to chemical engineering kinetics & reactor design*. John Wiley & Sons, Inc.

Holmes, H. F., and Gammage, R. B. (1975). "Interaction of gases with lunar materials: revised results for Apollo 11." *Proc. sixth Lunar Sci. Conf.*, 3343–3350.

ten Kate, I. L., Cardiff, E. H., Dworkin, J. P., Feng, S. H., Holmes, V., Malespin, C., Stern, J. G., Swindle, T. D., and Glavin, D. P. (2010). "VAPoR – Volatile Analysis by Pyrolysis of Regolith – an instrument for in situ detection of water, noble gases, and organics on the Moon." *Planet. Space Sci.*, 58(7–8), 1007–1017.

Kleinhenz, J. E., Sacksteder, K. R., and Nayagam, V. (2008). "Lunar Resource Utilization: development of a reactor for volatile extraction from regolith." *Proc. 46th AIAA Aerosp. Sci. Meet. Exhib.*

Kleinhenz, J., and Linne, D. (2013). "Preparation of a frozen regolith simulant bed for ISRU component testing in a vacuum chamber." *51st Aerosp. Sci. Conf.*

Lambert, J. M., Simkovich, G., and Walker, P. L. (1998). "The kinetics and mechanism of pyrite-to-pyrrhotite transformation." *Metall. Mater.*

*Trans. B*, 29B, 385–396.

Leybold GmbH. (2009). "Turbovac SL 80 incorporation declaration & operating instructions 130000760_002_A1."

Malvern Instruments. (2007). *Measurements of particle size distribution by wet & dry laser diffraction*.

Pitcher, C., Kömle, N., Leibniz, O., Morales-Calderon, O., Gao, Y., and Richter, L. (2016). "Investigation of the properties of icy lunar polar regolith simulants." *Adv. Sp. Res.*, 57(5), 1197–1208.

Poston, M. J., Grieves, G. A., Aleksandrov, A. B., Hibbitts, C. A., Darby Dyar, M., and Orlando, T. M. (2013). "Water interactions with micronized lunar surrogates JSC-1A and albite under ultra-high vacuum with application to lunar observations." *J. Geophys. Res. Planets*, 118(1), 105–115.

Reiss, P. (2018a). "A combined model of heat and mass transfer for the in situ extraction of volatile water from lunar regolith." *Icarus*, 306, 1–15.

Reiss, P. (2018b). "In-situ thermal extraction of volatiles from lunar regolith." Dissertation, Technical University of Munich.

Reiss, P., Hoehn, A., Walter, U., Barber, S., and Carpenter, J. (2017). "Implications of sample size for the thermal extraction of volatiles from lunar regolith with the PROSPECT instrument package." *J. Aerosp. Eng.*, 30(3), 04016088.

Rickman, D. L., and Lowers, H. A. (2012). *Particle shape and composition of NU-LHT-2M*.

Robens, E., Bischoff, A., Schreiber, A., Dabrowski, A., and Unger, K. K. (2007). "Investigation of surface properties of lunar regolith: Part I." *Appl. Surf. Sci.*, 253(13 SPEC. ISS.), 5709–5714.

Robens, E., Bischoff, A., Schreiber, A., and Unger, K. K. (2008). "Investigation of surface properties of lunar regolith - Part II." *J. Therm. Anal. Calorim.*, 94(3), 627–631.

Street, K. W., Ray, C., Rickman, D., and Scheiman, D. A. (2010). *Thermal properties of lunar regolith simulants*. *NASA/TM—2010-216348*, National Aeronautics and Space Administration.

U.S. Geological Survey. (2008). *Material safety data sheet NU-LHT-2M*.

Wright, I. P., Sheridan, S., Barber, S. J., Morgan, G. H., Andrews, D. J., and Morse, A. D. (2015). "CHO-bearing organic compounds at the surface of 67P/Churyumov-Gerasimenko revealed by Ptolemy." *Science (80-. ).*, 349(6247), aab0673-aab0673.

Zeng, X., He, C., and Wilkinson, A. (2010). "Geotechnical properties of NU-LHT-2M lunar highland simulant." *J. Aerosp. Eng.*, 23(4), 213–218.

# Highlights

- NU-LHT-2M was hydrated with water in mass fractions around 0.1 %
- In a ProSPA-like laboratory breadboard the water was extracted by heating
- NU-LHT-2M releases the added volatile water below a temperature of 300 °C
- Different sample conditions develop different characteristic gas pressures
- NU-LHT-2M releases trapped water, $CO_2$, and $H_2S$ from decomposition above 300 °C